Journal of Physics B:
Atomic, Molecular and
Optical Physics

PAPER

Vibrations of spherical nanoparticles

To cite this article: Tengfei Ying *et al* 2026 *J. Phys. B: At. Mol. Opt. Phys.* **59** 045101

Journal of Physics B: Atomic, Molecular and Optical Physics

PAPER

RECEIVED
23 November 2025

REVISED
8 February 2026

ACCEPTED FOR PUBLICATION
18 February 2026

PUBLISHED
26 February 2026

Vibrations of spherical nanoparticles

Tengfei Ying[1,4], **Xinyang Shu**[1,5] **and Klavs Hansen**[2,3,*]

[1] School of Science, Tianjin University, Tianjin 300072, People's Republic of China
[2] Center for Joint Quantum Studies and Department of Physics, School of Science, Tianjin University, Tianjin 300072, People's Republic of China
[3] Quantum Solid State Physics, Department of Physics and Astronomy, KU Leuven, 3001 Leuven, Belgium
[4] Present address: Thrust of Advanced Materials, Hong Kong University of Science and Technology (Guangzhou), Guangzhou 511453, People's Republic of China.
[5] Present address: State Key Laboratory of Surface Physics and Department of Physics, Fudan University, Shanghai 200433, People's Republic of China.
[*] Author to whom any correspondence should be addressed.

E-mail: klavshansen@tju.edu.cn

Keywords: vibrational modes, nanoparticles, vibrational angular momentum

Abstract

The vibrational modes of spherical monoatomic gas phase nanoparticles are calculated by quantizing the solutions of Lamb. The mode cutoff gives the two types of modes equal weights, and rounds the high frequency, both in strong contrast to Debye model spectra. The calculated spectra agree fairly well with spectra obtained by numerical diagonalization of Hessians of large disordered Lennard–Jones (LJ) clusters. The effect of a symmetry in the atomic arrangement is demonstrated with calculations for ground state LJ clusters. Our calculations allow the specification of the angular momentum carried by the vibrational motion, for which an example is calculated.

1. Introduction

The motion of the nuclei is the most important contribution to the thermodynamics of condensed matter over a wide range of temperatures, including those relevant for both production and applications of nanoparticles [1–3]. In gas phase the vibrational thermal properties play an essential role, not only for the thermal properties of clusters and small particles but also for the experimental characterization of other properties [4–6]. For the widely used technique known as action spectroscopy [7–9] the thermal properties are needed to extract the precise quantum yields, for example.

There are a few techniques available to obtain the vibrational spectra, understood as the collection of vibrational quantum energies $\hbar\omega$, of such particles. One is Fourier transform of velocity correlation functions in molecular dynamics simulations [10–12]. Such calculations and others of entirely numerical nature need to be performed case by case and tend not to provide any general insight into the topic. The present work aims at providing results that allow the calculation of vibrational spectra under conditions that are commonly encountered, based on the classical work of Lamb [13] on the vibrational modes of an elastic sphere.

A main feature of the normal modes of an elastic sphere is that reflections at the surface will mix the transverse and longitudinal waves [13]. This prevents the rigorous separation of transverse and longitudinal modes that greatly simplifies the solutions of the equations for bulk matter with the Debye model [14]. A separation can, however, be accomplished in terms of two other classes of modes. One contains the torsional (twisting) vibrations, i.e. those that do not cause deformations of a sphere. The other type of modes distort the shape of the surface and are denoted spheroidal vibrations. The equations of motion and solution were given by Lamb in 1881 [13]. Given by the time they were derived these equations describe the motion of continuous matter. The equations have found extensive use in the continuum description of planetary vibrations (see, e.g. [15]), and the equations have been extended to inhomogeneous density spheres [16], as well as spherical shells [17]. Recent work on water clusters include experiments on levitated micrometer sized droplets [18, 19]. Application to clusters include

[20], where a selection of modes were used to describe dynamics. In [21] an attempt of a full spectral analysis was given with what seems to us to be incorrect frequency cutoff values, however. The application given here to description of the complete vibrational spectra of particles composed of atoms is to the best of our knowledge not previously available in the literature.

Likewise, no analysis seems to be available in the literature of the angular momentum spectra associated with the vibrational motion. Characterizing a particle's angular momentum content is clearly important for chemical reactions by its nature as a conserved quantity. The connection between vibrational modes and angular momentum has been analyzed in, e.g. [22, 23]. For an example for generic liquid droplets, see [24], for helium droplets [25], and for linear molecules [26]. The interpretation of the classical deformations in terms of corresponding quantum numbers may encounter pitfalls, as pointed out by Dicke [27], but these difficulties seem not to be present here, and we can identify the integers l and m that appear in the derivations with the corresponding angular momentum quantum numbers (the standard notation for quantum mechanics is used here; the notation where l and n are exchanged was used by Lamb and others [13, 28, 29]).

The first aim of the present work is to determine the frequency cutoffs required for nanoparticles composed by atoms, and to use this to calculate the spectra. For nanoparticles composed of monomers which interact isotropically (simple particles) it is a reasonable proposition that vibrational spectra will possess some universally features that can be described fairly accurately with only a few material parameters. The material parameters here turn out to be the longitudinal and transverse speeds also known from the Debye theory. For such simple particles, the results here should therefore be a universal good first approach. The second aim is to give expressions for vibrational angular momentum.

In the remainder of the article we will introduce the required frequency cutoffs after a brief review of the fundamental equations, and use the cutoffs to give the frequency spectra of both nanoparticles and the smaller Ångström particles of clusters that can still be described as spherical. Expressions for the angular momentum distributions are then calculated and an example given. The analytical work will be tested against numerically calculated spectra of clusters composed of monomers interacting through the Lennard–Jones (LJ) potential, and an unanticipated effect of geometric symmetry demonstrated.

2. Characterizing the modes

The equations of motion and their solutions in the continuum limit can be found in [28–30]. The solutions provide the starting point for the work here and we will review the relevant results here briefly. The modes involve the shear modulus μ, the mass density ρ, the constant $\lambda \equiv E\nu/(1+\nu)(1-2\nu)$ which is one of the Lamé constants, Young's modulus E, and ν, the dimensionless Poisson ratio, i.e. the ratio of lateral contraction to longitudinal extension when a bar of the substance is stretched. The parameters λ, μ, and E all have units of energy per volume. The solutions for the modes involve the two speeds

$$C_1 \equiv \left((\lambda + 2\mu)/\rho\right)^{1/2}, \tag{1}$$

and

$$C_2 \equiv (\mu/\rho)^{1/2} = (E/2\rho(1+\nu))^{1/2}, \tag{2}$$

corresponding to the longitudinal and transverse speeds, respectively, of the material. The values are independent of the shape of the particle, and can therefore be found from experiments on bulk matter.

The solutions to the equations of motion are divided into torsional and spheroidal modes. With a particle radius of a the scaled torsional mode frequencies are given by the equation [31]

$$(l-1)\, j_l(K_2 a) - K_2 a j_{l+1}(K_2 a) = 0, \quad l = 0, 1, 2, \ldots, \tag{3}$$

with j_l the spherical Bessel functions. The roots of equation (3), $x_{l,n}$, are labeled with l and the counting index n, then give the torsional frequency spectrum

$$\omega_{l,n} = x_{l,n} C_2 / a. \tag{4}$$

There are two special cases. The case $l = 0, m = 0$ describes a static sphere. The other is $l = 1$, with $m = 0, \pm 1$, which describe rotations of the sphere around the three axes [13].

The spectrum of frequencies up to 100, i.e. $x \leqslant 100 \Rightarrow \omega_{l,n} \leqslant 100\ C_2/a$, is plotted in figure 1. The figure suggests an approximately quadratic spectrum for the torsional vibrations. This is also the dependence derived from the asymptotic behavior of the solutions.

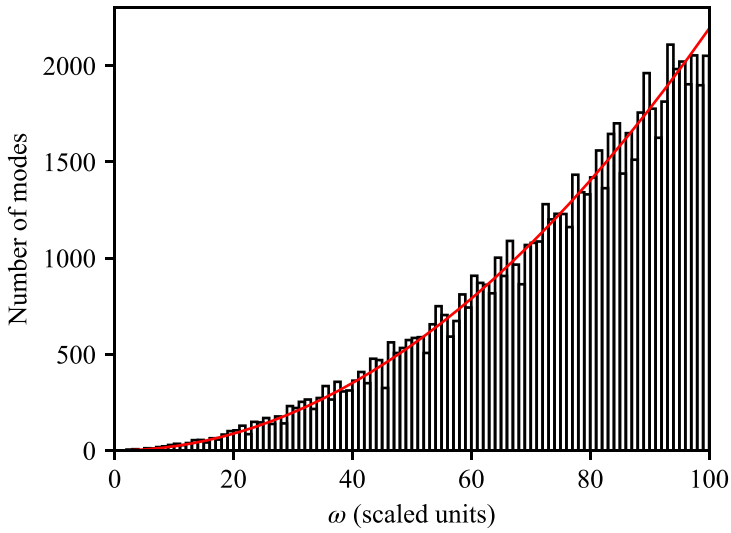

Figure 1. The frequency spectrum of torsional vibrations found by a direct calculation of the zeros of equation (3). The line shows the fitted quadratic dependence $0.217\omega^2$, which is in reasonable agreement with the asymptotically large ω coefficient of $0.202\omega^2$ from equation (8).

The leading order asymptotic form of the spectrum is found by considering the asymptotics of the Bessel functions in the frequency equation:

$$(l-1)\frac{1}{x_{l,n}}\cos\left(x_{l,n}-\frac{(l+1)\pi}{2}\right)-\cos\left(x_{l,n}-\frac{(l+2)\pi}{2}\right)=0, \tag{5}$$

or, including only the last, leading order term,

$$x_{l,n}\approx\left(\frac{l}{2}+n\right)\pi. \tag{6}$$

There is therefore a degeneracy for modes where l changes by ±2 and n simultaneously by ∓1. With the degeneracy of $2l+1$ for each l this gives the total number of states

$$\rho_{\text{torsional}}(\omega)=\frac{1}{2}\sum_{l=0}^{l_{\max}}(2l+1)=\frac{1}{2}(l_{\max}+1)^2. \tag{7}$$

From equation (6) we have $l_{max}=2\omega/\pi$. This gives the asymptotic spectrum

$$\rho_{\text{torsional}}(\omega)\approx\frac{2}{\pi^2}\omega^2. \tag{8}$$

The quadratic dependence agrees with the form found in figure 1, with the numerical constant close to the asymptotic value. The torsional spectrum in figure 1 is universal in the sense that it depends only a single speed (C_2), with the concomitant dependence of this speed on material parameters.

Spheroidal vibrations, which distort the spherical shape, mix longitudinal and transverse waves and the spectra involve both speeds C_1, C_2. The solutions are found as functions of $K_1=\omega/C_2$ and the ratio C_1/C_2 with the equation [29]

$$\begin{aligned}&\left\{\left(l^2-l-\frac{1}{2}\eta^2\right)j_l\left(\eta\frac{C_1}{C_2}\right)+2\eta\frac{C_1}{C_2}j_{l+1}\left(\eta\frac{C_1}{C_2}\right)\right\}\left\{\left(l^2-1-\frac{1}{2}\eta^2\right)j_l(\eta)+\eta j_{l+1}(\eta)\right\}\\&-\{l(l+1)[(l-1)j_l(\eta)-\eta j_{l+1}(\eta)]\}\left\{(l-1)j_l\left(\eta\frac{C_1}{C_2}\right)-\eta\frac{C_1}{C_2}j_{l+1}\left(\eta\frac{C_1}{C_2}\right)\right\}=0.\end{aligned} \tag{9}$$

The socalled Poisson materials for which $\lambda=\mu$, have a Poisson's ratio $\nu=0.25$. This value is typical for many materials, suggesting moderate lateral expansion or contraction under axial loads. This gives $C_1/C_2=1/\sqrt{3}$.

A remark is in place for the $l=0$ modes. These modes are all breathing modes, i.e. they involve only radial vibration. The roots of equation (9) make one factor in the equation diverge at the center of the

particle. This invalidates the harmonic approximation and requires specific treatment of the atomic granularity at the center of the particle. Given the low statistical weight of these states (12 states out of a total of 3000 for $N = 10^3$, and 17 states for $N = 10^4$) we will summarily ignore the offending factor in the equation for these few modes.

Similarly to the torsional modes, there are three zero-frequency spheroidal modes, those with $l = 1, n = 1$. They correspond to a translation of the sphere as a whole. This completes the tally for the six non-vibrational degrees of freedom of a free non-linear particle.

3. Mode cutoffs

The determination of the high frequency cutoffs of the vibrational modes in a spherical particle is more intricate than for those of Debye particles. For a Debye model, cutoff frequencies are determined simply by the total number of modes together with their partition into two transverse types and one longitudinal with equal weights for the three types. This simple counting is not available for the modes of a sphere. In contrast to the Debye model the number of torsional and spheroidal modes are therefore not known *a priori*, only their total number of $3N-6$ for a free particle. It is therefore not justified to simply copy the procedure of the Debye model and set the number of modes to a ratio of 2:1. Neither will a simple ranking of vibrational frequencies and introducing the concomitant high value cutoff produce the correct spectrum. Another procedure where the n-value of the modes is disregarded and a cutoff based solely on the l-index as done in [21] appears equally incorrect.

A cutoff is instead implemented here by first adding the wave numbers for the two orthogonal displacements in square to determine the resulting wave numbers,

$$\kappa = \sqrt{\left(\frac{\pi n}{a}\right)^2 + \left(\frac{l}{a}\right)^2}. \tag{10}$$

The total spectrum is then given by the frequencies of the lowest $3N-6$ values of κ among both torsional and spheroidal modes, taking into account the $2l+1$ degeneracy. After the selection is made, the torsional and spheroidal spectra are rescaled with the values C_2/a and C_1/a, respectively.

This counting of modes is numerical and will in general require that a subset of the $2l+1$ degenerate modes of the highest frequency is selected. Small deviations from ideality for a real particle will provide a small splitting of the κ values, thus providing a natural selection of the relevant modes. The number of these modes is usually small and as small deviations from ideality will cause little scatter in this group of modes we can safely leave the issue at that.

The soundness of the procedure is confirmed by a calculation of the cutoff wave number, κ_0. Solving for the largest n for a given l with equation (10) gives

$$n = \frac{1}{\pi}\left(a^2\kappa_0^2 - l^2\right)^{1/2}. \tag{11}$$

The total number of modes, M, is then

$$M \approx \frac{1}{\pi}\int_0^{a\kappa_0} (2l+1)\left(a^2\kappa_0^2 = l^2\right)^{1/2} \mathrm{d}l = \frac{2}{3\pi}a^3\kappa_0^3. \tag{12}$$

Equating this to $3N$ and setting the particle radius equal to $a = r_1 N^{1/3}$ gives

$$\kappa_0 = \left(\frac{9\pi}{2}\right)^{1/3} r_1^{-1} \approx \frac{2.4}{r_1}. \tag{13}$$

This is independent of particle size N, as required, and it is also on the order of the reciprocal interatomic spacing. The coefficient $\approx$2.4 seems to be beyond the limit set by oversampling, but a comparison with the corresponding value for the Debye model shows a similar value. For argon the Debye temperature of 92 K and the longitudinal speed of sound of 950 m s^{-1} gives the value $\kappa_0 = 1.27 \times 10^{10}$ m^{-1}. The values of r_1 that gives the relation $a = r_1 N^{1/3}$ used above is found from the tabulated density of $\rho = 1.784$ g cm^{-3} as $r_1 = 3m_{\mathrm{Ar}}/4\pi\rho$ to the value 2.07 Å. The product $\kappa_0 r_1$ is then 2.6, in good agreement with the value 2.4 calculated.

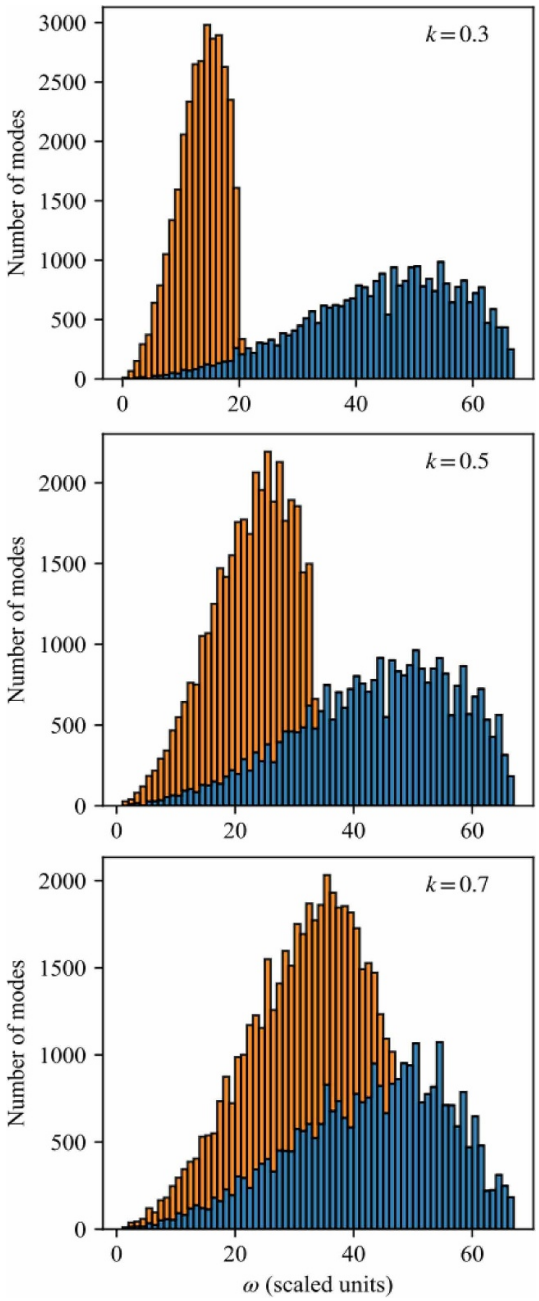

Figure 2. The vibrational spectra for $N = 10^4$ atoms for the three ratios of the two speeds $C_2/C_1 = 0.3, 0.5, 0.7$. The abscissas are scaled with C_1. The stacked red and blue columns are the torsional and spheroidal vibrational spectra, respectively.

4. Total spectra

Figure 2 shows the spectra calculated with the procedure described above for an $N = 10^4$ particle and $k \equiv C_2/C_1$ of 0.3, 0.5, 0.7, a range which covers most materials. (Tables of the frequencies for $k = 0.1$ through 1.0 in steps of 0.1 for the lowest 3×10^4 modes are available from the authors.) The contributions of the torsional and spheroidal modes to the total spectrum are both quadratic with frequency up to a smooth damping which sets in around 70% of the cutoff value. The number of modes of the two types is similar and the ratio of the two upper limits is close to the relative value of the two speeds. The slightly ragged shape of the spectra is caused by the high angular momentum degeneracy and the correspondingly small number of distinct energy levels, even for an $N = 10^4$ particle. For a realistic situation level distributions will be smeared, eliminating a good deal of the fluctuations, as seen in the numerical example for $N = 10^3$ shown below.

The contribution from both the torsional and the spheroidal modes have forms that, apart from the scaling of the abscissa, are approximately independent of the ratio C_2/C_1, as expected. Interpolation

between tabulated values for close$k$ values will therefore give a good approximation for intermediate value spectra.

A comparison with the results in [32] provides a perspective on the relevance of the calculations of particles as elastic spheres. The article shows numerical calculations of vibrational spectra of different particle sizes of monomers interacting with different potentials. The particles were all created with disordered geometries and devoid of the type of symmetry-induced peaks discussed below. The reported spectra in figures 10 and 11 of [32] show a striking tendency to universality across the type of interaction potential and particle sizes. The authors do not consider speed of sound, as would be needed to make statements of the spectra based on the analysis here, but we venture the guess that these potentials form particles with C_2/C_1-values clustered around 0.5, similarly to the real materials the potentials are supposed to mimic. The observed tendency to universality corroborates the universality conjecture made in the Introduction here.

5. Comparisons with numerical spectra

Experimental ground state vibrational spectra are not available in the literature, to the best of our knowledge. As a substitute we compare our results with simulated spectra of atomic nanoclusters. Figure 3 shows an example calculated for the ground state structure for the $N = 55, 400, 1000$ LJ clusters with the geometry available from [33]. The $N = 55$ is chosen for the comparison because it is a geometric shell closing. The spectrum is calculated with the standard procedure of determining the Hessian matrix and diagonalizing it, obtaining the frequencies as the square roots of the eigenvalues. Apart from the unsurprising smoothing of the spectrum compared to the spectrum of a similar size Lamb particle, the main difference is the presence of a prominent peak at $\omega \approx 10$, even visible in the fairly sparse spectrum for $N = 55$. The peak coincides with the dimer vibrational frequency of $\sim$10.69, although it is not clear if this is simply a numerical coincidence. The peak is clearly present irrespective of the cluster being a shell closing (as $N = 55$) or not ($N = 400, 1000$) in the ground state structures.

The origin of the peak was traced to the icosahedral symmetry of the particle which is present in the ground state structures for shell closings and open shells alike. This was demonstrated by generating quenched structures of glassy geometry. The structures were calculated by a rapid thermal quench of the structure of a particle excited above the melting point. The glassy nature of the structure is assigned by a comparison of the total potential energies of the quenched structures with the known ground state energies. Four spectra are shown in figure 4 for both $N = 300$ and $N = 1000$. These quenched spectra reproduce very well between structures, both for the different sizes and different quenches of the same size. The Debye spectrum shown in the inset is calculated for argon with the longitudinal and transverse speeds of 1528 and 736 m s^{-1}, respectively. They correspond to the two scaled Debye frequencies 37.0 and 17.8, calculated as the speeds multiplied by the ratio of LJ parameters $\sqrt{m/\epsilon} = \sqrt{40u/120\,\mathrm{K}}$ and by $\left(6\pi^2 N/V\right)^{1/3}$. The volume is calculated for a spherical particle with the radius given by $r = 35\langle d\rangle/36$, $\langle d\rangle$ being the average interatomic distance [34]. Comparison with the Lamb spectra in figure 2 suggest the value $C_1/C_2 \approx 0.6$, although remnants of the icosahedral symmetry could still influence the spectra. For comparison, the calculated ratio for LJ matter is very close to 0.5 around the melting point [35].

A spectrum with similar features as the icosahedral particle, viz. a sharp peak superposed on a broad and otherwise featureless part was also found for a $4 \times 6 \times 6$ NaCl cluster in [36]. The author ascribes the peak to unspecified short wavelength modes. Given the above results, we suggest instead that it arises as an effect the high symmetry of the crystallite structure, similar to the effect demonstrated in this work.

The heterogeneity of the shear elasticity of the glassy structure [37] is another factor that can potentially cause the simulated spectra to deviate that a Lamb spectrum. A comparison between the Lamb spectra and the simulated quenched spectra suggests that this does not have a significant influence, but the effect may be relevant for the transition from a Lamb spectrum to a Debye spectrum, as discussed briefly below.

Another interesting comparison of the above results is with the numerically calculated spectrum for the experimentally relevant Na^+_{139} of [4], made in [38] and shown in their figure 2. The spectrum was calculated for the optimized structure of a truncated icosahedron. The Poisson ratio of sodium at room temperature is 0.41 [39], corresponding to a $k = C_2/C_1$ of 0.39 and the relevant comparison here is then the frames for $k = 0.3$ and $k = 0.5$ in figure 2. The agreement is reasonable, given the caveats by the effects of the icosahedral symmetry already identified above. The abscissa scales in that work and the

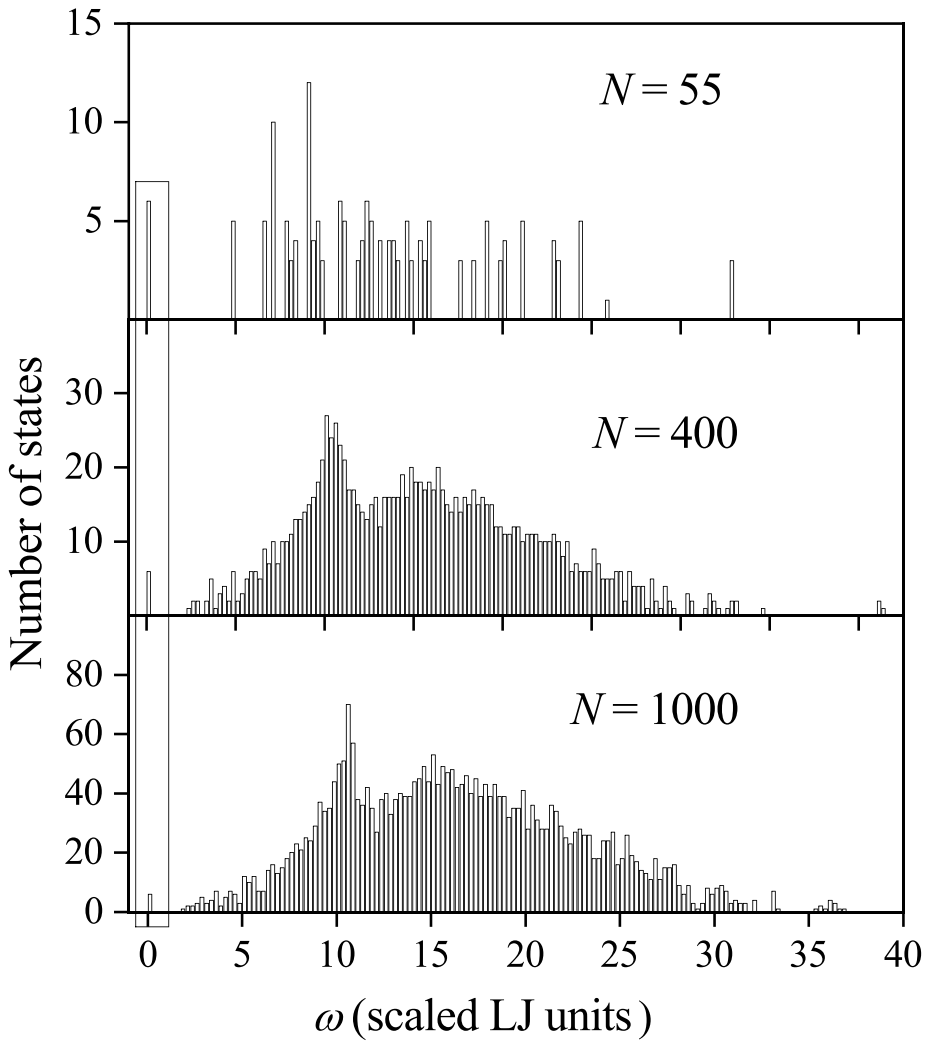

Figure 3. The vibrational spectra for the ground state of the $N = 55, 400, 1000$ Lennard–Jones clusters. Note that the scale on the Lamb spectra shown elsewhere and the LJ spectra shown here are not identical (the former includes the speed of sound C_1 and the latter involves the dimer frequency). The six zero frequencies of the translational and rotational motions are indicated by the box.

present can be compared directly, and also the ranges of the spectra compare reasonably. A longitudinal speed of 3200 m s^{-1} and a maximum wave vector calculated from the bulk density gives an upper spectrum cutoff at 130 cm^{-1}, not too different from the 150 cm^{-1} in the spectrum in [38].

A comment is in place for surface waves, called ripplons in helium droplets, where they account for a large part of the thermal excitation energy at the typical temperatures (≈0.4 K) of helium droplets flying freely in vacuum. The connection of these waves to the solutions given here has been found in [15] where it is shown that the $n = 1$ and $l > 0$ modes form these so-called Rayleigh surface waves. The figures of the radial distribution for $n = 1$ given in [29] provides a clear visualization of these waves.

6. Angular momenta

Quantization of the vibrational modes endows the angular part of their motion with angular momentum with the usual eigenvalues

$$L^2 = l(l+1)\hbar^2 \qquad l = 0, 1, 2\ldots, \tag{14}$$

and for the projection on the space-fixed z axis:

$$L_z = m\hbar \qquad m = 0, \pm 1, \pm 2, \ldots, \pm l. \tag{15}$$

The M_J (or K) quantum number arising for degeneracies of the rotational angular momentum of spherical particles [40] does not appear here.

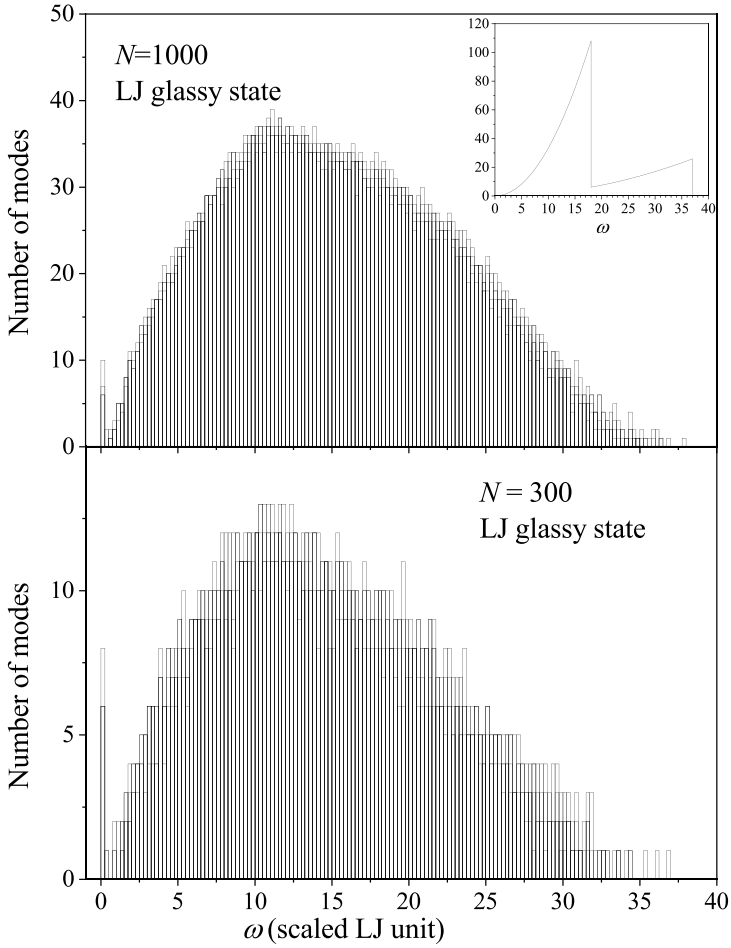

Figure 4. Four cases of the vibrational spectra for both $N = 300$ and $N = 1000$ quenched clusters of atoms interacting with the LJ potential. The inset in the top frame shows the corresponding Debye spectrum. The few extra apparent zero frequency are due to the finite size binning used.

The angular momentum distribution in a thermal population is calculated here for a canonical distribution, i.e. with a fixed temperature and particle number. The calculation proceeds through two steps. First the distribution of the projection of total angular momentum is calculated, following the procedure in [41] of random addition of the value for each mode. The number of angular momentum projections is distributed with the density

$$\rho(l_z) = \delta\left(l_z, \sum_{\{m_i\}}\sum_i \frac{1}{2l_i+1}\frac{m_i}{\mathrm{e}^{\hbar\omega_i/k_\mathrm{B}T}-1}\right), \tag{16}$$

where δ is the Kronecker delta, the sum over i runs over all modes, and the sum over $\{m_i\}$ is the sum over all combinations of m-quantum numbers of all modes. The fraction with the exponential is the probability that at least one quantum is present in the mode. Considering the number of terms in the averaging the distribution is expected to be Gaussian. This is borne out by a Monte Carlo simulation. The result for $N = 1000$ is shown in figure 5 for $T = 10$ in scaled units (to be compared with the upper edge of 67 in the middle spectrum in figure 2). Distributions for other temperatures with higher temperatures (not shown) have very similar widths and shapes. The angular momentum distribution is derived from the l_z distribution as [41]

$$\rho(l = l_z) = \rho(l_z - 1) - \rho(l_z). \tag{17}$$

Figure 6 shows this distribution for the input values used in figure 5.

The calculated example in this section gives a representative angular momentum distribution, but does not address its effect on its effects on unimolecular reactions and infrared optical activity where angular momentum conservation takes a prominent place. These topics are beyond the scope of this paper and will be deferred to another place.

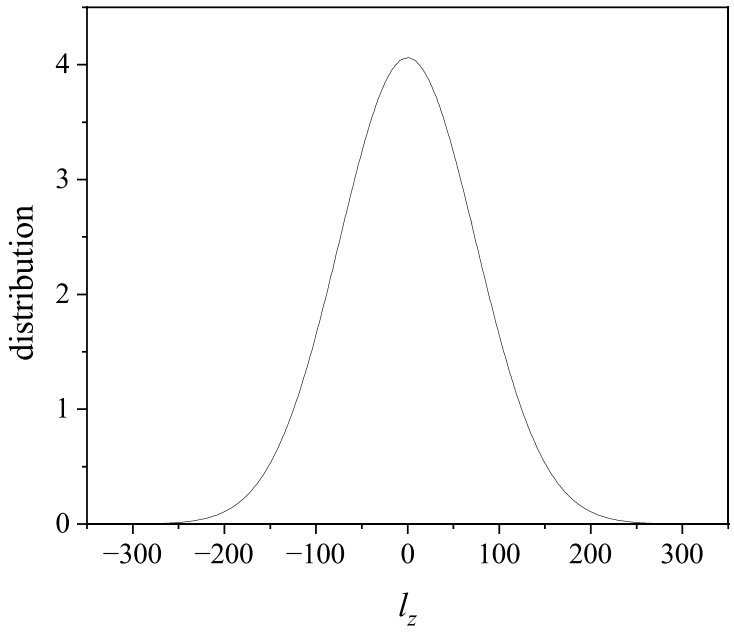

Figure 5. The distribution of the total projection of angular momentum for the states of a particle with $N = 1000$ and $C_2/C_1 = 0.5$ at the scaled unit temperature 10.

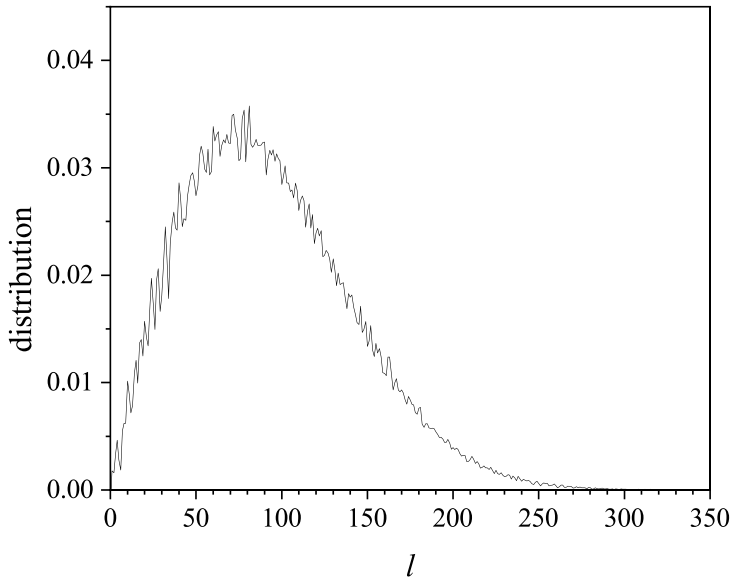

Figure 6. The distribution of the angular momentum derived from the curve in figure 5.

7. Discussion

The derivation here does not impose any restrictions on the size of a particle for the applicability of the results. Indeed, Lamb's classical results have also found applications for macroscopic objects [42]. The question naturally arises which objects have Lamb spectra and which should be described by Debye theory. The transition is expected to occur at a more or less well defined particle size, i.e. for a certain particle length scale. The quantization of the equations of motion made here introduce the interatomic spacing in addition to the radius of the particle as a length scale. The two length scales intrinsic to the derivation are the radii of the particles and the inter-atomic spacing. Neither of these two define the cross-over length scale, which therefore must be a length scale external to the theory developed so far.

We propose the phonon mean free path as the defining parameter. The main differences between Debye and Lamb theory is the mixing of polarizability modes at reflection at the surface in the latter. The importance of this mixing will be suppressed for particle sizes that are large compared with the

mean-free path of phonons. The ratio of phonon mean free path and particle radius therefore defines the transition from a Debye to a Lamb spectrum with decreasing particle sizes. As a potentially observable effect we note that as mean free paths change with temperature, this transition will potentially therefore also involve a transition of thermal properties with temperature for a given particle size. Both this thermal effect and the cross-over are observable quantities. The presence of the boson peak [37], ascribed to strong attenuation/short phonon mean free path in glassy materials, will potentially distort the cross-over from Lamb to Debye particles. In the simulations presented here the phenomenon is not seen.

8. Summary

This work provides the vibrational spectra of spherical monoatomic nanoparticles after adding the atomic granularity and the quantization of modes to the classical solutions of Lamb. As part of the process, the mode cutoff is established which gives the two types of modes equal weights. It rounds the high frequency end of the spectra. Calculated spectra show a strong contrast to Debye model spectra, and agree fairly well with numerically calculated spectra. The unanticipated effect of a geometric symmetry in the packing of the atoms appears with calculations of spectra of ground states of LJ clusters. The calculations allow the specification of the angular momentum carried by the vibrational motion, for which an example is calculated.

Data availability statement

The data cannot be made publicly available upon publication because no suitable repository exists for hosting data in this field of study. The data that support the findings of this study are available upon reasonable request from the authors.

Conflicts of interest

No conflicts of interest to declare.

Ethics statement

No ethics permission was required for this study.

Funding statement

No funding was used for this study.

Author contributions

Tengfei Ying 0009-0003-5292-4467
Formal analysis (equal), Methodology (equal), Software (equal), Visualization (equal)

Xinyang Shu
Formal analysis (equal), Investigation (equal), Software (equal)

Klavs Hansen 0000-0001-9746-3711
Conceptualization (equal), Data curation (equal), Investigation (equal), Methodology (equal), Project administration (equal), Supervision (equal), Validation (equal), Visualization (equal), Writing – original draft (equal), Writing – review & editing (equal)

References

[1] Roduner E 2006 Size matters: why nanomaterials are different *Chem. Soc. Rev.* **35** 583–92
[2] Selmani A, Kovačević D and Bohinc K 2022 Nanoparticles: from synthesis to applications and beyond *Adv. Colloid Interface Sci.* **303** 102640
[3] He G, Zhang X, Liu J, Chong J, Ye G and Fei H 2025 Hydrocarbothermal flow synthesis of carbon-supported small and dense high-entropy alloy nanoparticles as electrocatalysts *Nat. Commun.* **16** 8172
[4] Hock C, Schmidt M and v. Issendorff B 2011 Low-temperature caloric behavior of a free sodium nanoparticle *Phys. Rev. B* **84** 113401
[5] Ferrari P, Janssens E, Lievens P and Hansen K 2019 Radiative cooling of size-selected gas phase clusters *Int. Rev. Phys. Chem.* **38** 405–40

[6] Gatchell M and Zettergren H 2022 Open questions on the interaction dynamics of molecules and clusters in the gas phase *Commun. Chem.* **5** 28
[7] Hansen K 2018 Action spectroscopy of highly excited molecular ions in molecular beams *Int. J. Mass Spectrom.* **430** 14–21
[8] Zettergren H *etal* 2021 Roadmap on molecular dynamics in the gas phase *Eur. Phys. J. D* **75** 152
[9] Fielicke A 2023 Probing the binding and activation of small molecules by gas-phase transition metal clusters via IR spectroscopy *Chem. Soc. Rev.* **52** 3778–841
[10] Dickey J M and Paskin A 1970 Size and surface effects on the phonon properties of small particles *Phys. Rev. B* **1** 851–7
[11] Kristensen W D, Jensen E J and Cotterill R M J 1974 Thermodymanics of small clusters of atoms: a molecular dynamics simulation *J. Chem. Phys.* **80** 4161–9
[12] Ozaki Y, Ichihashi M and Kondow T 1992 Spheroidal and torsional vibrations of nearly spherical Ar clusters calculated by molecular dynamics *Chem. Phys. Lett.* **188** 555–9
[13] Lamb H 1881 On the vibrations of an elastic sphere *Proc. London Math. Soc.* **1–13** 189–212
[14] Ashcroft N W and Mermin N D 1976 *Solid State Physics* (Saunders College)
[15] Usami T and Satô Y 1964 Propagation of spheroidal disturbances on a homogeneous elastic sphere *Bull. Earthq. Res. Inst.* **42** 273–87
[16] Heyliger P R and Jilani A 1992 The free vibrations of inhomogeneous elastic cylinders and spheres *Int. J. Solids Struct.* **29** 2689–708
[17] Baker W E 1961 Axisymmetric modes of vibration of thin spherical shell *J. Acoust. Soc. Am.* **33** 1749–58
[18] Luo X, Zhou Z, Liu W, Shen D, Yan H, Lin Y and Wan W 2021 Vibrational modes in an optically levitated droplet *Opt. Lett.* **46** 4602–5
[19] Shah J R, Deshmukh D, Huisman M, Hanstorp D and Marmolejo J T Irradiation-driven evaporation of micro droplets in an optical trap (arXiv:2412.10784v1)
[20] Salzwedel R, Knorr A, Hoeing D, Lange H and Selig M 2023 Theory of radial oscillations in metal nanoparticles driven by optically induced electron density gradients *J. Chem. Phys.* **158** 064107
[21] Nishiguchi N and Sakuma T 1981 Vibrational spectrum and specific heat of fine particles *Solid State Commun.* **38** 1073–7
[22] Bohr A and Mottelson B R 1998 *Nuclear structure Vol.ii* (World Scientific Publishing)
[23] Landau L D and Lifshitz E M 1977 *Quantum Mechanics* 3rd edn (Pergamon)
[24] Tamura A and Ichinokawa T 1984 Liquid drop model of a small particle in a liquid state *Surf. Sci.* **136** 437–48
[25] Hansen K, Johnson M D and Kresin V V 2007 Density of states of helium droplets *Phys. Rev. B* **76** 235424
[26] Hansen K and Ferrari P 2021 Vibrational angular momentum level densities of linear molecules *Chem. Phys. Lett.* **768** 138385
[27] Dicke R H 1955 Angular Momentum of a Real Field *Phys. Rev.* **97** 536–9
[28] Pao Y-H and Mow C-C 1971 *Diffraction of Elastic waves and dynamic stress concentrations*
[29] Eringen A C and Şuhubi E S 1975 *Elastodynamics vol. 2, Linear Theory* (Academic)
[30] Sommerfeld A 2022 *Mechanics of deformable bodies* (Elsevier Inc)
[31] Hosseini-Hashemi S and Anderson J S 1988 Orthogonality and normalization of torsional modes of vibration of solid elastic spheres *J. Sound Vib.* **121** 511–24
[32] Matharoo G S, Sarkar S K and Pandey A 2005 Vibrational spectra of amorphous clusters: universal aspects *Phys. Rev. B* **72** 075401
[33] Wales D J, Doye J P K, Dullweber A, Hodges M P, Naumkin F Y, Calvo F, Hernández-Rojas J and Middleton T F The Cambridge Energy Landscape Database
[34] Hansen K 2025 Statistical physics of nanoparticles in the gas phase *Springer Series on Atomic, Optical and Plasma Physics* vol 128, 3rd edn (Springer)
[35] Khrapak S A 2020 Sound velocities of Lennard-Jones systems near the liquid-solid phase transition *Molecules* **25** 3498
[36] Martin T P 1983 Alkali halide clusters and microcrystals *Phys. Rep.* **95** 167–99
[37] Marruzzo A, Schirmacher W, Fratalocchi A and Ruocco G 2013 Heterogeneous shear elasticity of the glasses: the origin of the boson peak *Sci. Rep.* **3** 1407
[38] Sauceda H E, Jesús Pelayo J, Salazar F, Pérez L A and Garzón I L 2013 Vibrational spectrum, caloric curve, low-temperature heat capacity and Debye temperature of sodium clusters: the Na^{+}_{139} case *J. Phys. Chem. C* **117** 11393–8
[39] Wang M J, Chang J-Y, Wolfenstine J B and Sakamoto J 2020 Analysis of elastic, plastic and creep properties of sodium metal and implications for solid-state batteries *Materialia* **12** 100792
[40] Atkins P W and Friedman R S 1997 *Molecular Quantum Mechanics* 3rd edn (Oxford University Press)
[41] Bethe H A 1937 Nuclear physics B. nuclear dynamics, Theoretical *Rev. Mod. Phys.* **9** 69
[42] Bhattacharya J, Hanasoge S and Antia H M 2015 Frequency shifts of resonant modes of the Sun due to near-surface convective scattering *Astrophys. J.* **806** 246